Available online at www.sciencedirect.com

ScienceDirect

Energy Procedia 55 (2014) 77 – 84

Energy Procedia

4th International Conference on Silicon Photovoltaics, SiliconPV 2014

Dynamic photoluminescence lifetime imaging for injection-dependent lifetime measurements

Sandra Herlufsen[a], Karsten Bothe[a], Rolf Brendel[a,b], Jan Schmidt[a,b]

[a]*Institute for Solar Energy Research Hamelin (ISFH), Am Ohrberg 1, D-31860 Emmerthal, Germany*
[b]*Institute of Solid-State Physics, Leibniz University of Hanover (LUH), Appelstraße 2, 30167 Hannover, Germany*

Abstract

We investigate the impact of an injection-dependent carrier lifetime in crystalline silicon on dynamic photoluminescence lifetime imaging (dynamic PLI). Although the dynamic lifetime approach is a technique that evaluates the time-dependence of a quantity proportional to the excess carrier density, it is only weakly influenced by the injection-level dependence of the lifetime. The reason for the little impact is the fact that the evaluation of dynamic PLI measurements does not only involve the decay of the carrier density, as it is common for photoconductance decay measurements, but also the increase of the carrier density directly after switching on the excitation source. In this contribution, we present injection-dependent lifetime measurements that are acquired with the camera-based dynamic PLI technique. We find that the deviation of the actual steady-state carrier lifetime from the lifetime obtained with dynamic PLI is less than 20 % for a wide range of measurement conditions.

Peer-review under responsibility of the scientific committee of the SiliconPV 2014 conference

Keywords: photoluminescence; charge carrier lifetime; silicon

1. Introduction

Dynamic lifetime techniques have proven to be very useful for the investigation of the electrical quality of crystalline Si wafers and ingots utilizing the photoconductance, the free carrier emission or the photoluminescence emission of an optically excited Si sample. Since the carrier lifetime is extracted directly from the time dependence of a signal related to the excess carrier density, dynamic techniques have the advantage of being independent of sample variations that impact the steady-state signal e.g. the optical properties of the sample surfaces, the doping density or the sample thickness. However, a major assumption for the correct determination of the steady-state carrier lifetime from a time-dependent quantity proportional to the excess carrier density is that the carrier lifetime is *independent* of the injection level. Figure 1 (a) shows the time-dependent excess carrier density for a square-wave

Peer-review under responsibility of the scientific committee of the SiliconPV 2014 conference
doi:10.1016/j.egypro.2014.08.081

shaped photogeneration rate (black line) with the carrier lifetime τ_{stst} as time constant (blue line). Additionally, we show the time-dependent excess carrier density for an injection-dependent lifetime (red line). During the variation of the excess carrier density over time, the carriers have different lifetimes according to the injection-dependent lifetime curve shown in Fig. 1 (b).

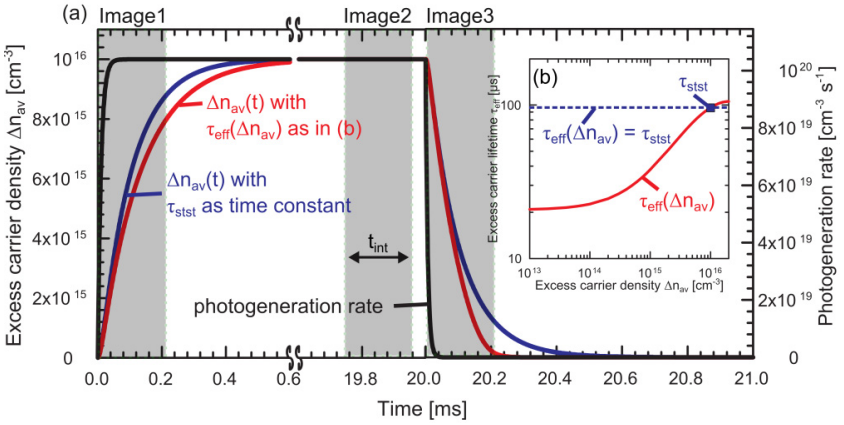

Fig. 1. (a) Time-dependent photogeneration rate and excess carrier density Δn(t) in case of an injection-independent carrier lifetime (blue) and in case of an injection-dependent lifetime (red). The gray bars mark the times of the image acquisition for dynamic PLI with the width being the camera integration time t_{int}. (b) Injection-dependent effective carrier lifetime $\tau_{eff}(\Delta n)$ that is used for the calculation of (a).

The impact of an injection-dependent lifetime can be reduced by narrowing the evaluated injection range as for photoconductance decay measurements [3]. Unfortunately, this is not applicable for dynamic photoluminescence lifetime imaging (dynamic PLI) measurements since the measurement interval is typically chosen in the order of the carrier lifetime to obtain a sufficiently high signal-to-noise ratio [1, 2]. Thus, the measurements are performed over a broad injection range. However, since the dynamic PLI approach evaluates not only the decay of the carrier density after an excitation source is switched off but also the increase of the carrier density directly after switching on the excitation source, it is possible that the impact of an injection-dependent lifetime cancels out. Ramspeck et al. [4] investigated the impact of an injection-dependent lifetime for dynamic infrared lifetime mapping (dynamic ILM) for an injection-dependent lifetime that is mainly dominated by defect recombination. They found that the impact on the measured dynamic ILM lifetime is negligible (below 30% deviation from the actual steady-state carrier lifetime).

In this contribution, we analyze the impact of an injection-dependent lifetime on the dynamic PL lifetime taking the quadratic dependence of the PL emission on the excess carrier density into account. We compare dynamic PL lifetime measurements with the actual carrier lifetime that is determined with a photoconductance-based steady-state lifetime technique. We demonstrate the reduced impact of an injection-dependent lifetime on the dynamic PL lifetime analysis for two important cases: (a) an injection-dependent lifetime limited by defect recombination and (b) an injection-dependent lifetime limited by Auger recombination. In addition, we perform numerical simulations of the dynamic PL lifetime to identify the most optimal measurement conditions.

2. Injection-dependent dynamic PL carrier lifetime measurements

2.1. Dynamic photoluminescence lifetime imaging

On the basis of measurements of the free carrier emission using an infrared camera, Ramspeck et al. [4, 5] introduced the dynamic infrared lifetime mapping (dynamic ILM) technique. They acquired three images at different times during a modulated excitation and showed that a ratio of these three images only depends on the camera integration time t_{int} and the effective carrier lifetime τ_{eff}. The measurement intervals for the three images are shown in Fig. 1 as gray bars with the width being the camera integration time. The increasing Δn(t) is recorded in

the first image and the decreasing Δn(t) in the third image. The second image is a steady-state image that is acquired in a time domain where Δn(t) is constant. Assuming a linear dependence between measured signal and excess carrier density S ~ Δn, Ramspeck et al. integrated the time-dependent excess carrier density over time and calculated the image ratio P [4]:

$$P = \frac{S_{Image1} - S_{Image3}}{S_{Image2}} = \frac{t_{int} + 2\tau_{eff}\exp(-t_{int}/\tau_{eff}) - 2\tau_{eff}}{t_{int}} \quad (1)$$

Using Eq. (1), the spatially resolved carrier lifetime can be easily extracted from a measured image ratio by comparing the experimentally determined signal ratio with the simulated ratio for every image pixel. We adapted the ILM approach to measurements of the PL emission and demonstrated the validity of Eq. (1) for the quadratic dependence of the PL emission on the excess carrier density [1, 2]. The main advantages of the dynamic PL approach over the ILM approach are a weaker impact of trapping and depletion region modulation [6] and that the lifetime measurement can be easily performed at room temperature.

We use a complementary metal oxide semiconductor (CMOS) indium gallium arsenide (InGaAs) camera for the detection of the luminescence emission. The excess carriers in the wafers are generated by a high power diode laser with a central wavelength of λ_{exc} = 805 nm. We use the light source in a pulsed mode using a rectangular pulse shape and a modulation frequency of 15 Hz. The required precise timing of the image acquisition is achieved by a TTL trigger signal that is send to the camera synchronously with the laser pulse.

2.2. Samples

Figure 2 (a) shows the injection-dependent lifetime of a 1 Ωcm boron-doped Cz-Si wafer that is passivated on both surfaces with a stack of Al_2O_3 and SiN_x. The injection dependence of the carrier lifetime is attributed to the boron-oxygen defect that is activated through illumination [7]. Figure 3 (a) shows the injection-dependent lifetime of a 240 Ωcm boron-doped FZ-Si wafer with an Al_2O_3 surface passivation on both surfaces. In this case, the injection dependence of the carrier lifetime is mainly due to radiative and Auger recombination. We determined the injection-dependent effective carrier lifetime for both samples with the dynamic PLI approach [1] and for comparison with the quasi-steady-state photoconductance technique (QSSPC) [8] and with photoconductance-calibrated PL imaging (PC-PLI) [9]. The FZ-Si sample is additionally investigated by photoconductance decay measurements (PCD) [2]. In addition to photogeneration rate and injection density, we vary the measurement interval of the dynamic PL lifetime measurement. This interval is equal to the camera integration time and determines which part of the injection dependence is actually detected. Both samples have a size of 5×5 cm^2. The PL lifetime images are averaged over the detection area of the PC-based lifetime setup to enable the comparison of the lifetime techniques.

2.3. Measurement conditions

The range of the accessible camera integration times is determined on the one hand by a sufficient signal-to-noise ratio (SNR) of the acquired signal and on the other hand by the maximum amount of photons that the detector is able to collect. Regarding the SNR, we found an optimum t_{int} value that is about three times the effective carrier lifetime τ_{eff} for our measurement setup [1]. However, a wide range of chosen t_{int} values yields a sufficiently high SNR, being advantageous since τ_{eff} is not known initially. The uncertainty of the dynamic PL lifetime is calculated by using the statistical uncertainties of the single PL images of the image ratio P in Eq. (1). We chose t_{int} to reach a statistical lifetime uncertainty below 5%. To obtain the carrier lifetime from the dynamic PL image ratio P, the difference between the steady-state PL image (Image2) and the images that are acquired during the increase or decrease of the PL emission (Image1 and Image3) has to be larger than the statistical uncertainty. For that reason, the number of averages has to be increased for $t_{int} << \tau_{eff}$ and $t_{int} >> \tau_{eff}$ to achieve a low statistical uncertainty. For our measurements, we accept a maximum number of averages of 10000.

An additional restriction is given due to the non-rectangular switching of the excitation source. For our laser, we

found laser-power-dependent switching time constants with a maximum value of about 10 µs for the highest laser power. The non-instantaneous switching of the excitation source is considered for the calculation of the dynamic PL image ratio by using a time-dependent photogeneration rate for determining the time-dependent excess carrier density (similar to Ref. 4). For the accurate determination of the carrier lifetime, the exact knowledge of the switching time constants is required. We measured the switching time constants by using a calibrated short-circuited reference solar cell. We estimated the uncertainty of the measured switching time constants to be ±1 µs to determine the lifetime uncertainty if using camera integration times in the order of the switching time constants (t_{int} < 100 µs).

2.4. Dynamic PL lifetime measurements

In Figs. 2 (a) and 3 (a), the steady-state lifetime techniques and the dynamic PLI approach are in excellent agreement for both injection dependencies. Figures 2 (b), (c), (d) and 3 (b), (c) and (d) present the measured dynamic PL lifetimes for a given photogeneration rate as a function of the camera integration time (red open squares). The error bars are the sum of the statistical uncertainty (that is kept minimized by increasing the number of averages) and the additional uncertainty due to the measured switching time constants of the laser (only significant for t_{int} < 100 µs). The gray, solid lines show the variation of the dynamic PL lifetime due to the injection-dependent lifetime from numerical simulations, assuming that the photoconductance-based lifetime measurements represent the actual steady-state carrier lifetimes. Furthermore, we take the injection-dependent coefficient of radiative recombination into account that describes the decreasing probability of radiative recombination with increasing injection density [10]. The gray dashed lines are modeled by assuming a 10% uncertainty of the PC-based lifetime measurement [11].

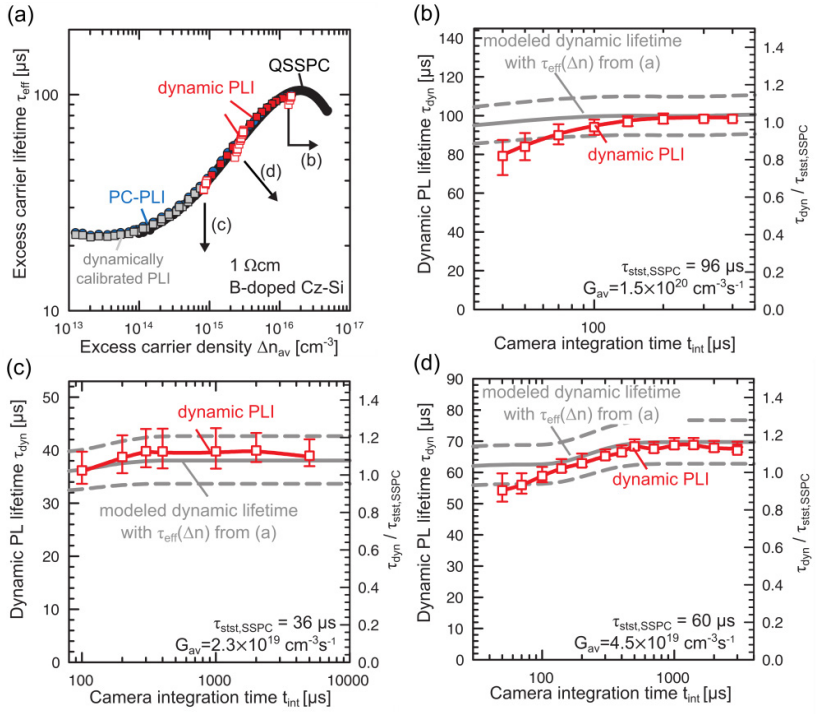

Fig. 2. (a) Injection-dependent lifetime of a 1 Ωcm B-doped Cz-Si wafer acquired using different lifetime measurement techniques. (b), (c) and (d) Dynamic PL lifetime τ_{dyn} as a function of the camera integration time t_{int} for the wafer of (a) and three different average photogeneration rates G_{av} [associated with the marked data points in (a)]. The gray, solid lines show the variation of the dynamic PL lifetime due to the injection-dependent lifetime from numerical simulations, assuming that the photoconductance-based lifetime measurements represent the actual steady-state carrier lifetimes. The gray dashed lines are modeled by assuming a 10% uncertainty of the PC-based lifetime measurement.

A variation of τ_{dyn} with camera integration time is expected since the camera integration time determines which part of the injection dependency is detected in Image1 and Image3. However, the measured deviation is below 20% since the impact of the injection-dependent lifetime is cancelled to a large extent by subtracting Image3 from Image1. For the lowly-doped FZ-Si wafer, it is noticeable that there seems to be an additional systematic difference between the PC-based and the dynamic PLI measurement that may be the result from uncertainties of the calibration of the PC setup [12]. Nevertheless, we can conclude that for an injection-dependent lifetime where the lifetime varies by about one order of magnitude, the choice of the measurement interval has a negligible impact on the measured dynamic PL lifetime.

The dynamic PL lifetime imaging technique is less sensitive towards low injection densities than a steady-state PL technique since the camera integration time t_{int} has to be in order of τ_{eff} whereas for a steady-state PL measurement, t_{int} can be adjusted to obtain a sufficient signal with a high SNR. For that reason, we did not perform dynamic PLI measurements for the low Δn ranges of Fig. 2 (a) and 3 (a). In that case, a PL calibration with the dynamic PL lifetime measurements is a valid approach to obtain the lifetimes in that low Δn and thus low signal regime. The dynamically calibrated lifetimes are displayed as gray squares in Figs. 2 (a) and 3 (a).

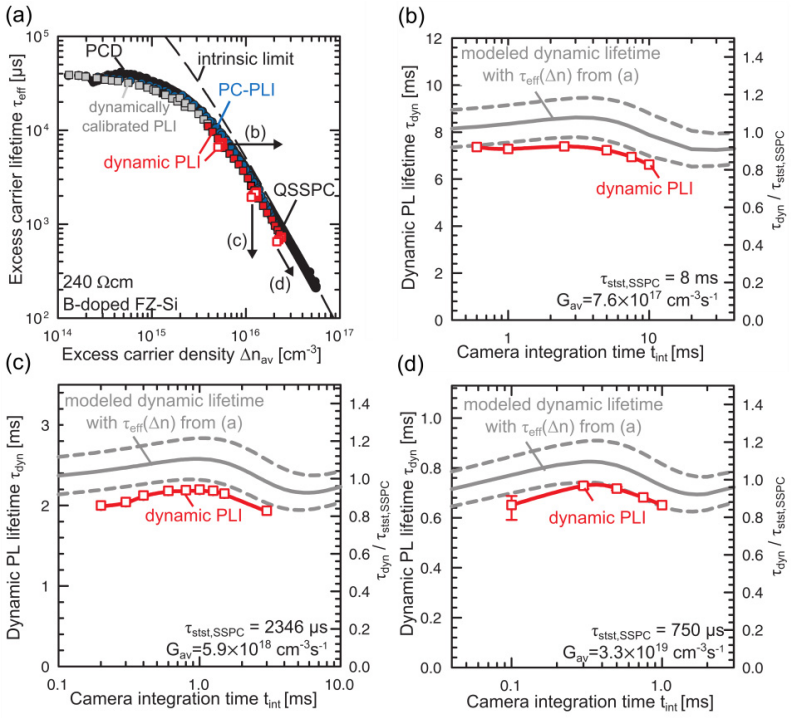

Fig. 3. Injection-dependent lifetime of a 240 Ωcm B-doped FZ-Si wafer acquired using different lifetime measurement techniques. (b) and (c) Dynamic PL lifetime τ_{dyn} as a function of the camera integration time t_{int} for the wafer of (a) and two different average photogeneration rates G_{av} [associated with the marked data points in (a)]. The gray, solid lines show the variation of the dynamic PL lifetime due to the injection-dependent lifetime from numerical simulations, assuming that the photoconductance-based lifetime measurements represent the actual steady-state carrier lifetimes. The gray dashed lines are modeled by assuming a 10% uncertainty of the PC-based lifetime measurement.

3. Simulations

For the study of the impact of an injection-dependent lifetime on dynamic PL lifetime measurements, we numerically determine the dynamic PL lifetime as a function of the camera integration time. At first, we extend the investigation of the injection-dependent lifetime with an increasing lifetime with injection density. We use the Shockley-Read-Hall model [13, 14], assuming a defect with an energy level of 0.3 eV above the valence band edge

and a constant capture cross section for holes of $\sigma_p = 2\times10^{-16}$ cm^2. We vary the ratio of the capture cross section for electrons and holes, the asymmetry factor $k = \sigma_n/\sigma_p$, from 10 to 1000. Figure 4 (a) shows the injection-dependent lifetimes that are used for our dynamic PL lifetime simulation. Figure 4 (b) presents the modeled dynamic PL lifetime as a function of the camera integration time with respect to the actual steady-state carrier lifetime τ_{stst}. The dynamic PL lifetime is evaluated at an injection density of $\Delta n_{eval} = 10^{16}$ cm^{-3}. For the modeling, we assumed an ideal light source with a square-wave shaped excitation.

For the defect-related injection dependence of the carrier lifetime, we observe only a small impact on the dynamic PL lifetime. The maximum deviations from the actual lifetime are below 15% for the highest asymmetry factor of 1000. This finding is consistent with the results of Ramspeck et al. who modeled the dynamic ILM lifetime for a linear dependence of signal and excess carrier density and could not find a deviation larger than 30% for any set of SRH parameters [4]. For $t_{int} >> \tau_{eff}$, the ratio τ_{dyn}/τ_{eff} becomes constant since the information of the single images of the dynamic PL image ratio P becomes constant. If we decrease the capture cross section of the holes σ_p and thus the magnitude of the carrier lifetime at an injection density of 10^{16} cm^{-3}, we observe a shift of τ_{dyn}/τ_{eff} to larger camera integration times. However, the maximum possible deviation from the actual carrier lifetime is only slightly influenced by a variation of σ_p.

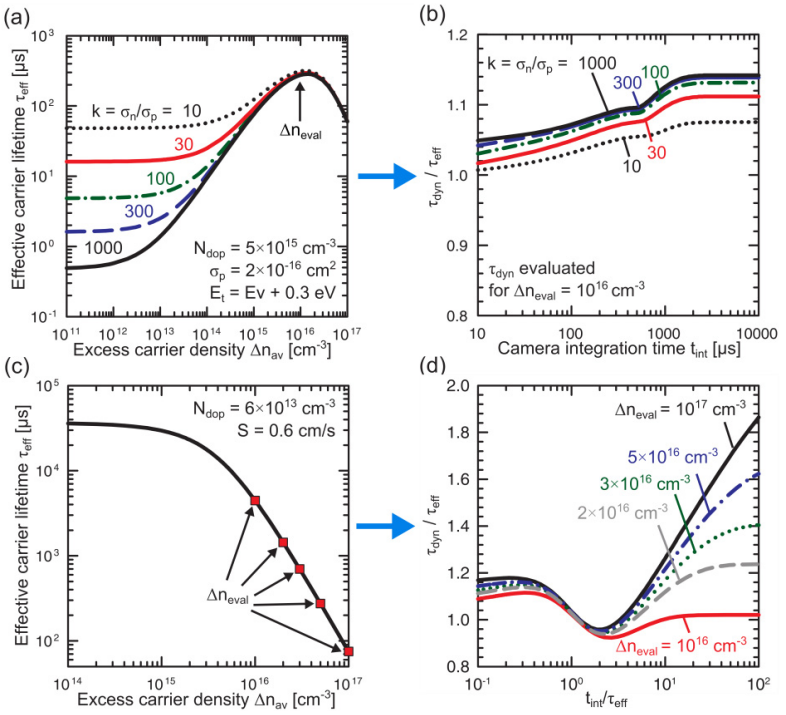

Fig. 4. (a) Injection-dependent lifetime for different asymmetry factors k. (b) Ratio of the modeled dynamic PL lifetime τ_{dyn} to the actual effective lifetime τ_{eff}. The dynamic PL lifetime is modeled as a function of the camera integration time t_{int} at an injection density of $\Delta n = 10^{16}$ cm^{-3} for the injection-dependent lifetimes of a. (c) Injection-dependent lifetime, limited mainly by radiative and Auger recombination for a wafer with a thickness of 300 µm, a doping density of 6×10^{13} cm^{-3} and a surface recombination velocity of 0.6 cm/s. (d) Ratio of the modeled dynamic PL lifetime τ_{dyn} to the actual effective lifetime τ_{eff} as a function of the camera integration time t_{int} for different injection densities.

Figure 4 (c) presents basically the injection-dependent lifetime that we measured on the lowly-doped FZ-Si wafer and that is shown in Fig. 3 (a). This is already an extreme case of an injection-dependent lifetime with a decreasing lifetime with injection density. For the modeling of the carrier lifetime, we assumed only intrinsic recombination and a surface recombination velocity of 0.6 cm/s (for a wafer thickness of 300 µm).

Similarly to Fig. 4 (b), we present the modeled dynamic PL lifetime as a function of the camera integration time. However, we normalize both axes to the actual effective carrier lifetime. For injection densities below 2×10^{16} cm^{-3}, we observe only small deviations between dynamic PL and actual lifetimes regardless the choice of the camera integration time $t_{int.}$ For injection densities larger than 2×10^{16} cm^{-3} we modeled higher deviations, especially for $t_{int} >> \tau_{eff}$. The reason for the increased ratio τ_{dyn}/τ_{eff} is the increasing difference between the steady-state lifetime at the evaluated Δn and the lifetime at low injection densities. We identified the third image (Image3 in Fig. 1) as the one with the strongest impact on the deviating dynamic PL lifetime. The high lifetimes at low injection densities result in a slowly-vanishing signal contribution that impacts the dynamic PL lifetime for long camera integration times. Thus, it is crucial to choose t_{int} in the order of τ_{eff} for the case of a decreasing τ_{eff} with increasing injection density. For the case of Fig. 4 (a), the situation is different since the short lifetimes at low injection densities result in a fast decaying excess carrier density in the sample.

Note, that in the considered case for the lifetime measurement at high injection densities, the quadratic dependence of the PL signal has a positive side effect since the steady-state signal is much higher than the slowly decaying low-injection signal contribution that is responsible for the deviation between actual and dynamic lifetime. The same injection dependence at low injection conditions would yield a much higher deviation from the actual steady-state carrier lifetime due to the linear relation between excess carrier density and PL emission at low injection densities.

We conclude that for injection densities below 2×10^{16} cm^{-3}, the deviation between actual steady-state carrier lifetime and dynamic PL lifetime is generally in the range of 20 %. For larger Δn, t_{int} has to be chosen in the order of the carrier lifetime ($t_{int}/\tau_{eff} < 10$) to avoid deviations from the actual steady-state carrier lifetime with dynamic PL lifetime measurements.

4. Conclusions

We were able to determine the actual steady-state carrier lifetime of silicon wafers with dynamic photoluminescence lifetime imaging with an uncertainty below 20% over a wide range of camera integration times. In this study, we have investigated two samples showing fundamentally different injection-dependent lifetime behavior. The first sample was a defect-recombination-limited Cz-Si wafer and the second sample a FZ-Si wafer that was limited by Auger recombination in the high-injection range. Additionally, we performed numerical simulations and found for extremely high asymmetry factors of k = 1000 a maximum deviation to the actual carrier lifetime of 15%. In case of a decreasing lifetime with increasing injection density, we identified deviations below 20% for t_{int} in the order of the carrier lifetime ($t_{int} < 10\tau_{eff}$).

Acknowledgements

This work was funded by the German State of Lower Saxony and the German Federal Ministry for the Environment, Nature Conservation, and Nuclear Safety and by industry partners within the research cluster “SolarWinS” (Contract No. 0325270E). The content is the responsibility of the authors.

The authors would like to thank Conny Marquardt and Dominic Walter from ISFH for the preparation of the investigated Si wafers.

References

[1] S. Herlufsen, K. Ramspeck, D. Hinken, A. Schmidt, J. Müller, K. Bothe, J. Schmidt, and R. Brendel, „Dynamic lifetime imaging based on photoluminescence measurements”, Proceedings of the 25th European Photovoltaic Solar Energy Conference, Valencia, Spain, 2010, pp. 2369-2373.

[2] S. Herlufsen, K. Ramspeck, D. Hinken, A. Schmidt, J. Müller, K. Bothe, J. Schmidt, and R. Brendel, „Dynamic photoluminescence lifetime imaging for the characterisation of silicon wafers“,Physica status solidi (RRL) 5, 25-27 (2011).

[3] H. Nagel, C. Berge, and A.G. Aberle, "Generalized analysis of quasi-steady-state and quasi-transient measurements of carrier lifetimes in semiconductors", Journal of Applied Physics 86, 6218-6221 (1999).

[4] K. Ramspeck, K. Bothe, J. Schmidt, and R. Brendel, “Combined dynamic and steady-state infrared camera based carrier lifetime imaging of silicon wafers”, Journal of Applied Physics 106, 114506 (2009).
[5] K. Ramspeck, S. Reissenweber, J. Schmidt, K. Bothe, and R. Brendel, „Dynamic carrier lifetime imaging of silicon wafers using an infrared-camera-based approach“, Applied Physics Letters 93, 102104 (2008).
[6] R. A. Bardos, T. Trupke, M. C. Schubert, and T. Roth, Trapping artifacts in quasi-steady-state photoluminescence and photoconductance lifetime measurements on silicon wafers, Applied Physics Letters 88, 053504 (2006).
[7] K. Bothe, J. Schmidt, "Electronically activated boron-oxygen-related recombination centers in crystalline silicon", Journal of Applied Physics 99, 013701 (2006).
[8] R. Sinton, A. Cuevas, "Contactless determination of current-voltage characteristics and minority-carrier lifetimes in semiconductors from quasi-steady-state photoconductance data", Applied Physics Letters 69, 2510-2512 (1996).
[9] S. Herlufsen, J. Schmidt, D. Hinken, K. Bothe, and R. Brendel, "Photoconductance-calibrated photoluminescence lifetime imaging of crystalline silicon", Physica status solidi (RRL) 2, 245-247 (2008).
[10] P. P. Altermatt, F. Geelhaar, T. Trupke, X. Dai, A. Neisser, and E. Daub, “Injection dependence of spontaneous radiative recombination in c-Si: experiment, theoretical analysis, and simulation”, Proceedings of the 5th international conference on numerical simulation of optoelectronic devices, Berlin, Germany, 2005, pp. 47-48.
[11] A. L. Blum et al., “Interlaboratory study of eddy-current measurement of excess-carrier recombination lifetime“, IEEE Journal of Photovoltaics 4, 525-531 (20134).
[12] K. R. McIntosh, J. Guo, M. D. Abbott, and R. A. Bardos, “Calibration of the WCT-100 photoconductance instrument at low conductance”, Progress in Photovoltaics 16, 279-287 (2008).
[13] W. Shockley and W. T. Hall, “Statistics and recombinations of holes and electrons”, Physical Review 87, 835-842 (1952).
[14] R. N. Hall, “Electron-hole recombination in germanium”, Physical Review 87, p. 387 (1952).